Intermetallics 107 (2019) 47–52

Contents lists available at ScienceDirect

Intermetallics

journal homepage: www.elsevier.com/locate/intermet

Preparation of non-magnetic and ductile Co-based bulk metallic glasses with high GFA and hardness

Guoyang Zhang[a,b,c], Hua Zhang[a,b,**], Shiqiang Yue[a,b], Rijin Cheng[a,b], Anding Wang[c,d,*], Aina He[c], Yaqiang Dong[c], Hongwei Ni[a,b], Chain-Tsuan Liu[d]

[a] The State Key Laboratory of Refractories and Metallurgy, Wuhan University of Science and Technology, Wuhan, 430081, China
[b] Key Laboratory for Ferrous Metallurgy and Resources Utilization of Ministry Education, Wuhan University of Science and Technology, Wuhan, 430081, China
[c] CAS Key Laboratory of Magnetic Materials and Devices, Zhejiang Province Key Laboratory of Magnetic Materials and Application Technology, Ningbo Institute of Materials Technology and Engineering, Chinese Academy of Sciences, Ningbo, Zhejiang, 315201, China
[d] Department of Materials Science and Engineering, College of Science and Engineering, City University of Hong Kong, Kowloon, Hong Kong, China

ARTICLE INFO

Keywords:
Bulk metallic glasses
Glass-forming ability
Mechanical properties
Magnetic properties
Crystallization phase

ABSTRACT

Co(Fe,Ni)-based bulk metallic glasses (BMGs) characterized with super-high hardness and strength are generally brittle and strong magnetic, significantly undercutting their momentous applications as coating materials. Here we report $Co_{92-x}Ni_2Ta_6B_x$ (x = 29–35) non-magnetic BMGs with a combination of appropriate plasticity and GFA, as well as superhigh hardness and strength. BMG Rods with maximum diameters up to 2.5 mm were fabricated by copper mold casting method. All alloys exhibit superhigh compressive fracture strength of 5.21–5.63 GPa, high hardness of 1290–1410 HV and plasticity of 1.2–3.5%. Besides, the amorphization can effectively decrease the magnetization and all the alloys show non-magnetic properties at glassy state. The partial crystallization in the high B content glassy alloys will not significantly change the non-magnetic or poor-magnetic feature. It is also found that the increase of B content can substantially improve the thermal stability of the glassy alloys and inhibit the formation of strong magnetic phases. These Co-based alloys are promising candidates for the future application of spray coating materials.

1. Introduction

Due to the absence of dislocation and grain boundary, the bulk metallic glasses (BMGs) show outstanding mechanical, physical and chemical properties, including superior strength, hardness, anticorrosion, wear resistance, soft-magnetic properties and so on, in comparison with the crystalline counterparts [1]. Significant interests have been attracted from various application fields and many alloy systems with exceptional properties have been developed after decades of research. Among the alloy community, the low cost Co(Fe,Ni)-based BMGs are most attractive for approaching the upper limits of soft-magnetic property and strength [2,3]. Beside the application as soft-magnetic ribbons and powders with low GFA requirement, the spray coating is another application field of a high prospective which can overcome the GFA determined size limit and highlight the advantages of high strength, hardness and corrosion resistance [4–6]. Nevertheless, the documented Co(Fe,Ni)-based BMGs are mostly ferromagnetic [7] and suffered from the ductile deformation due to the strength-plasticity trade-off [8]. It is quite desired to develop non-magnetic or weak-magnetic BMGs to eliminate the magnetic disturbance of the coating [9].

In consideration of the required properties for coating application, it is worth to analyze first from the two main production processes [10]: powder preparation and coating spray (as shown in Fig. 1) [11,12]. It has been accepted that the cooling rate of the powder atomization devices is about 1–2 orders of magnitude lower than the copper roller melt-spinning process [13]. The cooling rate of the molten powders by the substrate in a coating spray process is also lower. Therefore, a certain GFA of 1–2 mm evaluated by copper mold casting is always needed for producing fully glassy powders and coatings [10]. The alloys closed to the eutectic point exhibiting high melt fluidity and low melting temperature are also preferred for increasing the sphericity of powders, decreasing the powder size distribution and the defects in the coating [14]. High strength and hardness are the basic requirement and

* Corresponding author. CAS Key Laboratory of Magnetic Materials and Devices, Zhejiang Province Key Laboratory of Magnetic Materials and Application Technology, Ningbo Institute of Materials Technology and Engineering, Chinese Academy of Sciences, Ningbo, Zhejiang, 315201, China.
** Corresponding author. The State Key Laboratory of Refractories and Metallurgy, Wuhan University of Science and Technology, Wuhan, 430081, China.
E-mail addresses: anding.w@hotmail.com (H. Zhang), anding@nimte.ac.cn (A. Wang).

https://doi.org/10.1016/j.intermet.2019.01.012
Received 13 October 2018; Received in revised form 8 December 2018; Accepted 10 January 2019

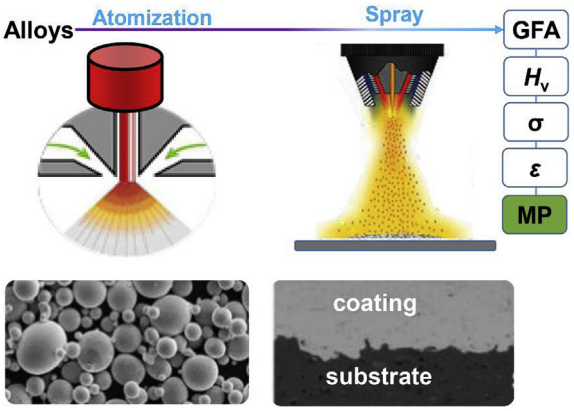

Fig. 1. Schematic diagram of the coating process and property requirements of alloys [9].

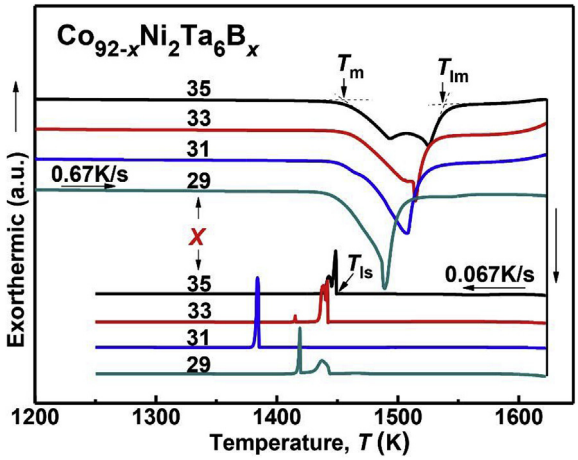

Fig. 2. DSC curves of the $Co_{92-x}Ni_2Ta_6B_x$ (x = 35, 33, 31, 29) master alloys showing the melting and solidification processes.

mainly determined by the alloy system [15]. Among the BMG community, the Co-based BMGs are found to exhibit highest strength and hardness, therefore be chosen in this study. Inoue et al. developed the ultrahigh-strength materials of CoFeTaB BMGs with the compressive fracture strength (σ) over 5000 MPa [8]. Wang et al. developed the CoTaB alloys which enhanced strength to 6000 MPa [16]. These alloys are found to be strong-yet-brittle and prone to catastrophic fracture, which needs more investigations to enhance the plasticity (ε_p) [17,18]. In addition, previous studies were mainly focused on the improvement of mechanic properties [15,19], GFA and magnetic properties, and very little attention has been paid to develop non-magnetic alloys. Development of alloy with saturate magnetic flux density (B_s) closed to zero is hence one of the key points considered in this study.

In this study, $Co_{92-x}Ni_2Ta_6B_x$ (x = 29–35) non-magnetic BMGs were developed, via Ni introduction for improving corrosion resistance and GFA as well as Co/B content adjustment, based on the $Co_{59}Ta_6B_{35}$ prototype alloy [16], The GFA, thermal stability, crystallization and solidification behaviors, mechanic and magnetic properties were investigated in details. Combinedly high performance containing high GFA up to 2.5 mm evaluated by copper mold casting method, superhigh compressive fracture strength of 5.21–5.63 GPa, high hardness of 1290–1410 HV, large plasticity of 1.2–3.5% and low B_s closed to zero were readily obtained. The $Co_{92-x}Ni_2Ta_6B_x$ (x = 29–35) non-magnetic glassy alloys with high performance are promising coating materials for industrial applications and important references for future development.

2. Experiment procedures

Co-Ta pre-alloy was first prepared by arc melting the mixture of pure Co (99.95 wt.%), Ta (99.95 wt.%) metals under a Ti-getterd high-purity argon atmosphere. $Co_{92-x}Ni_2Ta_6B_x$ (x = 35, 33, 31, 29) alloy ingots with the nominal composition were prepared by induction melting with the mixture of Ni (99.99 wt.%), B (99.5 wt.%) and Co-Ta pre-alloy in a high purity argon atmosphere. Melt-spinning technique and copper mold casting method were used to produce the glassy ribbons and cylindrical rods, respectively. The ribbons with a width of 1.2–1.3 mm and thickness of 20–24 μm were prepared by a single roller at the wheel speed 40 m/s in an argon atmosphere.

The microstructure of ribbon and rod samples was investigated by X-ray diffraction (XRD) with Cu-Kα radiation. The melting and solidification behaviors of master alloys were analyzed by differential scanning calorimetry (DSC) at a heating rate of 0.67 K/s and low cooling rate of 0.067 K/s to reduce the effect of undercooling, to accurately obtain the intrinsic melting temperature (T_m), liquidus temperatures (T_{lm} and T_{ls}). The thermal properties of glassy alloys were identified by DSC at a heating rate of 0.67 K/s, by using the metal-spun ribbons with a fully glassy structure. The compression test using cylindrical rods (1 mm in diameter and 2 mm in length) was performed with a universal testing machine at the strain rate range of 5×10^{-4}-5×10^{-2} s^{-1}. The Vickers hardness (HV) measurement was conducted on the 1 mm diameter rod samples under a load of 5 N for 10 s. After mechanical tests, deformation and fracture morphologies were observed by scanning electron microscopy (SEM). B_s was measured with a vibrating sample magnetometer (VSM) under a field of 800 A/m.

3. Results and discussion

3.1. Thermal properties and glass-forming ability

Melting and solidification processes of the $Co_{92-x}Ni_2Ta_6B_x$ (x = 35, 33, 31, 29) master alloys were firstly investigated by DSC and shown in Fig. 2. The T_m and T_{lm} masked on the heating section show the onset and offset temperatures of the melting endothermic events. It is clear that the T_m and T_{lm} increase gradually with the increase of B content and the two melting peaks split more clearly. The T_{ls} denoted in the cooling section showing the onset temperature of the solidification exothermic event. The $Co_{61}Ni_2Ta_6B_{31}$ alloy exhibits only one crystallization peak and the lowest T_{ls}, suggesting the approaching of the eutectic point. Other alloys exhibit two split crystallization peaks correlated to two crystallization processes and are off-eutectic compositions [2,20].

The DSC curves of the as-spun $Co_{92-x}Ni_2Ta_6B_x$ (x = 35, 33, 31, 29) glassy ribbons at a heating rate of 0.67 K/s are shown in Fig. 3. Before crystallization, distinct glass transition followed by a wide supercooled liquid region can be observed. With the increase of B content, the glass transition temperature (T_g) increases gradually from 893 K to 940 K and the onset temperature of crystallization (T_x) increases faster from 916 K to 980 K. As a result, the supercooling liquid region (ΔT_x) increases from 23 K to 40 K. It is also clear that the difference of specific heat (ΔH) at the glass transition region increase drastically, suggesting that the high B content alloys exhibit higher thermal stability of supercooled liquid [21]. The increase of B content also decreases the number and temperature interval of the crystallization peaks, indicating the changes of precipitation phases. It should be noted that the T_x of these alloys is over 900 K which is much higher than other alloy systems, enables high thermal stability and crystallization resistance during coating production processes [21].

Copper mold casting method was then employed to evaluate the GFA of these $Co_{92-x}Ni_2Ta_6B_x$ (x = 35, 33, 31, 29) alloys, by casting rod samples with diameters (D) of 1–3 mm. Fig. 4 shows the XRD patterns of $Co_{57+x}Ni_2Ta_6B_{35-x}$ (x = 0, 2, 4, 6) alloy rods with critical diameters

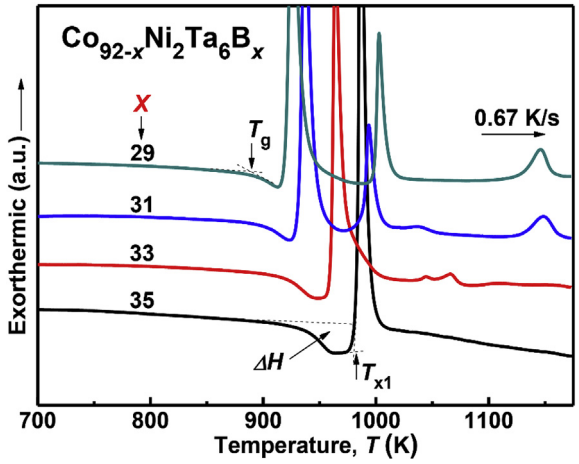

Fig. 3. DSC curves of the as-spun $Co_{92-x}Ni_2Ta_6B_x$ (x = 35, 33, 31, 29) glassy alloys.

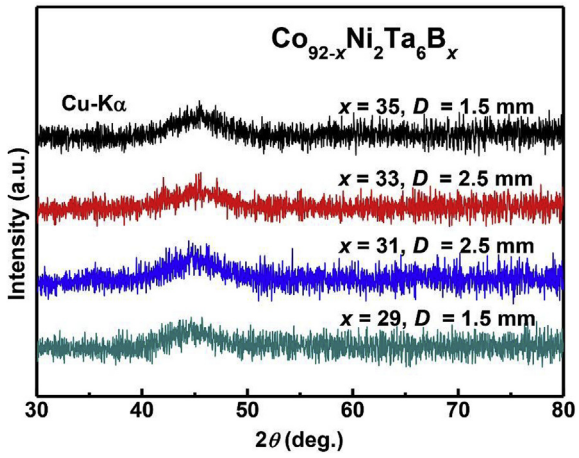

Fig. 4. XRD patterns of the as-cast $Co_{92-x}Ni_2Ta_6B_x$ (x = 35, 33, 31, 29) alloy rods with diameters of 1.5, 2.5, 2.5 and 1.5 mm, respectively.

(D_c) of 1.5, 2.5, 2.5 and 1.5 mm, respectively. Only broad peaks without any apparent crystalline Bragg peak can be seen from the patterns, indicating the fully glassy structure of these samples within the resolution of the X-ray measurement conditions. Compared with the basic $Co_{59}Ta_6B_{35}$ alloy, GFA of $Co_{92-x}Ni_2Ta_6B_x$ (x = 35, 33, 31, 29) alloys is readily improved via Ni introduction and B content adjustment in a large range, which can guarantee the glassy structure and manufacturability of the coating.

Based on the thermal parameters, we did a simple theoretical analysis of GFA [22], by using the commonly used criterions [23] including a supercooled liquid region ($\Delta T_x = T_x - T_g$), reduced glass transition temperature ($T_{rg} = T_g/T_{ls}$) and γ parameter ($\gamma = T_x/(T_g + T_{ls})$). The thermal characteristic temperatures, GFA criterions and D_c are shown in Table 1. The dependences of the GFA criterions and experimentally obtained D_c on B content show substantial differences, stressing the importance of evaluation by casting. The deviations of the calculated criterions and D_c have been well reported in other BMG alloy systems [18–20], interpreting in terms of the limitations of criterions and the influence of measurement methods of the thermal parameters, and etc. It is accepted that the GFA of an alloy is depended on multiple thermodynamic and kinetic factors [20,21]. The empirical GFA criterions are proposed with different assumptions and simplifications, thereby can not be applied in the $Co_{92-x}Ni_2Ta_6B_x$ (x = 35, 33, 31, 29) alloys. The GFA change with B content is most believably explained for the eutectic composition theory. As shown in Fig. 2, the alloys with x = 33 and 31 are closed to the deep eutectic point and exhibit the highest GFA. It should be noted that all alloys exhibit high T_{rg} and γ, compared with other Co-based, Fe-based FeNi-based and FeCo-based alloys with high GFA [19]. The large Co and B content ranges are very important for ensuring BMG formation in the industrial melting with large composition fluctuation.

3.2. Mechanical properties

The indentation experiment can provide valuable information about the mechanical behavior of brittle materials such as BMGs [24]. Fig. 5 shows the Vickers indentations obtained under a load of 5 N for 10 s. All the BMG samples show similar creak free patterns and well-developed slip-steps around the indents, suggesting the good ductility. The number of shear bands increases and then decreases with the decrease of B content, and all of the BMGs shows the good microscopic plasticity. Comparative study of the much larger indentation area of 304 stainless steel clearly exhibits the super-high hardness of 1290–1410 HV (listed in Table 2). Since the hardness can directly reflect the wear resistance [25,26], the $Co_{92-x}Ni_2Ta_6B_x$ (x = 35, 33, 31, 29) glassy alloys have great potential to be good coating materials.

In order to further explore the mechanical properties of $Co_{92-x}Ni_2Ta_6B_x$ (x = 35, 33, 31, 29) alloys, uniaxial compression test was taken at room temperature. Fig. 6 presents the compressive stress-strain curves for the rod samples with a diameter of 1 mm. All curves show a distinct plastic deformation with work-hardening behavior and dense serrations after yield, implying the continuous initiation of multiple shear bands with different critical shear stress in different regions [27]. Although the σ_y and σ_c decrease gradually with the decrease of B content, all BMGs exhibit ultrahigh yield strength (σ_y) of 5.08–5.48 GPa and compressive fracture strength (σ_c) of 5.21–5.63 GPa, as listed in Table 2. It is clear that the yield strength (σ_y), fracture strength (σ_c) and Vickness hardness (HV) of the alloys can be tuned synchronously by adjusting the B content. It is noted that the plasticity (ε_p) of this superhigh strength alloy can be well improved from 1.2% to 3.5% by adjusting the Co and B contents. More detailed evaluation of the deformability in practical application [28], the compression test of $Co_{61}Ni_2Ta_6B_{31}$ BMG rods was also conducted at higher strain rates up to $5 \times 10^{-2}\ s^{-1}$. Although the plastic strain decreases with the increase of strain rate, the glassy alloy still maintains a appreciate plasticity, as shown in Fig. 6. Since it has been proved that the plasticity has severe dimension effect and can be significantly improved by decreasing the size [29,30], the coating made with the ductile $Co_{92-x}Ni_2Ta_6B_x$ (x = 35, 33, 31, 29) alloys is prone to exhibit better plastic performance.

As well proved, deformation and fracture surfaces can reflect the mechanical behaviors of BMGs in a compression test [31]. $Co_{63}Ni_2Ta_6B_{29}$ BMG specimens after deformation and fracture were

Table 1
The thermal parameters, GFA criterions and critical diameters of $Co_{92-x}Ni_2Ta_6B_x$ (x = 35, 33, 31, 29) alloys.

Alloys	T_g (K)	T_x (K)	T_m (K)	T_{ls} (K)	ΔT_x (K)	T_{rg}	γ	D_c (mm)
$Co_{57}Ni_2Ta_6B_{35}$	940	980	1449	1449	40	0.649	0.410	1.5
$Co_{59}Ni_2Ta_6B_{33}$	920	958	1456	1442	38	0.638	0.406	2.5
$Co_{61}Ni_2Ta_6B_{31}$	901	928	1449	1385	27	0.651	0.406	2.5
$Co_{63}Ni_2Ta_6B_{29}$	893	916	1444	1444	23	0.618	0.392	1.5

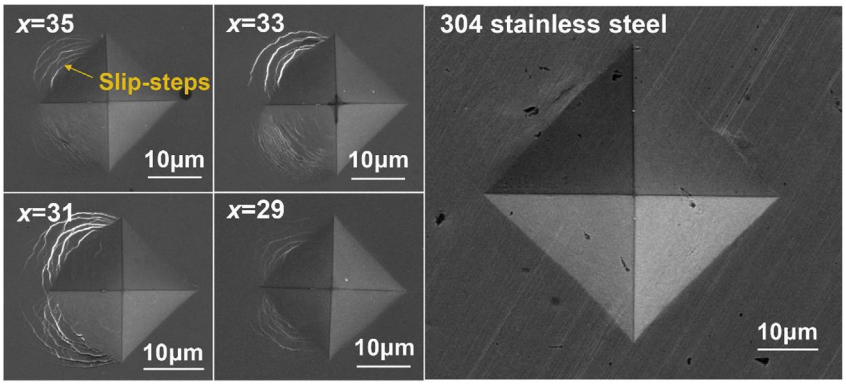

Fig. 5. SEM images of Vickers indentations of the as-cast $Co_{92-x}Ni_2Ta_6B_x$ (x = 35, 33, 31, 29) BMGs and 304 stainless steel under a load of 5 N for 10 s.

Table 2
The mechanical properties of as-cast $Co_{92-x}Ni_2Ta_6B_x$ (x = 35, 33, 31, 29) BMG rods tested with strain rate of 5×10^{-4} s^{-1}.

Alloys	ρ (g/cm^3)	HV	σ_y (GPa)	σ_c (GPa)	ε_p (%)
$Co_{57}Ni_2Ta_6B_{35}$	8.95	1410	5.48	5.63	1.2
$Co_{59}Ni_2Ta_6B_{33}$	9.00	1380	5.17	5.36	1.7
$Co_{61}Ni_2Ta_6B_{31}$	9.05	1330	5.15	5.31	2.3
$Co_{63}Ni_2Ta_6B_{29}$	9.11	1290	5.08	5.21	3.5
304 stainless steel	7.91	380	0.31	–	–

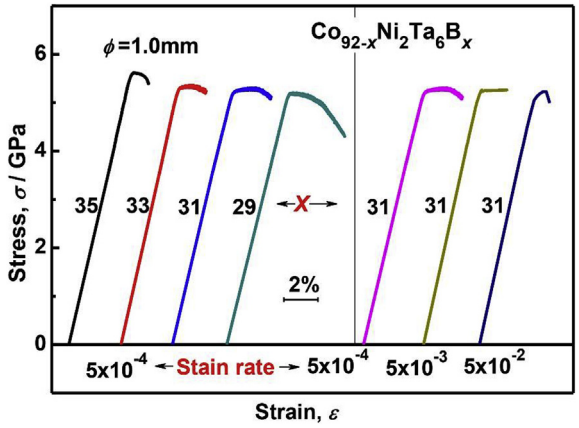

Fig. 6. Compressive stress–strain curves of $Co_{92-x}Ni_2Ta_6B_x$ (x = 35, 33, 31, 29) glassy rods tested with different strain rate.

selected for SEM observation, to deeper understand the high plasticity. Fig. 7a displays the lateral surface morphology of the BMG rod unloaded after about 2% plastic strain before fracture. Multiple shear bands can be observed on the deformed sample surface as enlarged in Fig. 7b. We can see that the shear angle between the primary shear band and the compressive axis is about 44° which is coincident to the former reports [31], demonstrating that the shear deformation is mainly controlled by the primary shear stress [32]. Fig. 7c shows the small fragments after drastic burst fracture which releases the high elastic energy. Apart from the cleavage-like patterns on most fracture surfaces which is the typical fracture feature of strong and brittle metallic glasses [31], vein-like patterns combined with melted liquid flows and droplets characterized of plastic deformation [27] were also found and shown in Fig. 7d and f. Fig. 7e shows the cleavage-like patterns of the fracture surface [33]. As enlarged in Fig. 7g, the fracture surface consists of typical mirror, mist and hackle regions [34]. Nanoscale homogenous parallel stripes in Fig. 7h was also found in the mirror region.

The high strength and hardness values of the current $Co_{92-x}Ni_2Ta_6B_x$ (x = 35, 33, 31, 29) BMGs can be interpreted to originate from strong bonding nature among the constituent elements as is expected from the mixing enthalpies with large negative values for Co–Ta, Ta–B and Co–B pairs [26,27,35]. The B content dependence of strength and hardness can also be explained by the change of bonding nature of metal–metal bonds and metal–metalloid bonds [36,37]. For the improvement of plasticity, it is speculated to stem from the Ni introduction and decrease of B content. In addition, the change of primary crystallization phase from complicated $(Co,Ta)_{23}B_6$ phase to simple phases studied in the

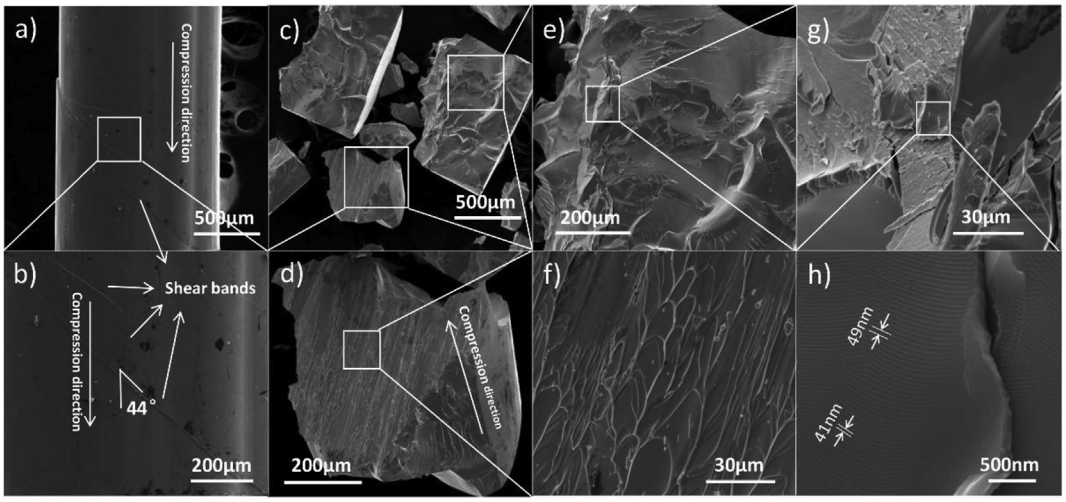

Fig. 7. SEM images of the deformed and fractured $Co_{92-x}Ni_2Ta_6B_x$ (x = 35, 33, 31, 29) BMG rods.

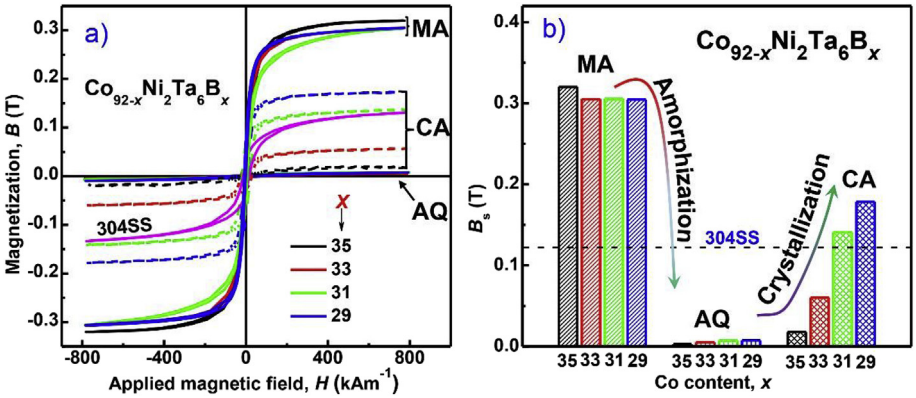

Fig. 8. Hysteresis B-H loops of $Co_{92-x}Ni_2Ta_6B_x$ (x = 35, 33, 31, 29) master alloys (MA), as-quenched (AQ) and crystallized alloy (CA) ribbons.

following part will also conduce to the formation of clusters which is crucial for ductile BMGs.

3.3. Magnetic properties

Magnetic properties are the crucial points of this study and for coating materials. Since the amorphicity of the powder and coating depended on atomization and spay processes would greatly affect the magnetic properties, all master alloy (MA), as-quenched (AQ) and crystallized alloy (CA) ribbons were measured by applying a field up to 800 kA. As shown in Fig. 8a, all MAs exhibit strong-magnetic hysteresis B-H loops with B_s values of about 0.3 T. But for the AQ ribbons, the B_s for all alloys keeps extremely low values less than 0.01 T, showing the non-magnetic feature. When we annealed the glassy ribbons over T_{x1} at 1073 K for 1 h, the low B content CA samples recover the strong-magnetic feature due to precipitation of crystalline phases. As depicted in Fig. 8b, the B and Co contents have poor influences on the B_s of the MA and AQ samples, while affects the B_s of the CA samples obviously. We note that the amorphization can effectively decrease the magnetization and lead to non-magnetic glassy alloys. It is also important that it is feasible to decrease the B_s of the CA samples by adjusting the Co and B contents. The partial crystallization in the $Co_{57}Ni_2Ta_6B_{35}$ glassy alloy will not significantly change the non-magnetic or poor-magnetic feature. Compared with the commonly used 304SS, the B_s of the $Co_{92-x}Ni_2Ta_6B_x$ (x = 35, 33, 31, 29) BMGs is much lower, even for the high B alloy samples with partial crystallization. All these results clearly verify the successful preparation of non-magnetic and ductile bulk metallic glasses with high GFA and hardness.

3.4. Crystallization behavior

In order to thoroughly understand the origin of high GFA and the B content influence on magnetic properties of $Co_{92-x}Ni_2Ta_6B_x$ (x = 35, 33, 31, 29) amorphous alloys the crystallization behavior and phases were investigated by employing an XRD. The annealing temperature was determined according to the DSC curves in Fig. 3. For the $Co_{92-x}Ni_2Ta_6B_{29}$ glassy alloy with three crystallization exothermic peaks, three samples annealed at different temperature were identified to unveil the structure evolution process. According to the patterns of samples annealed at 916 K (T_x) and 961 K in Fig. 9, the initial precipitation of the $Co_{63}Ni_2Ta_6B_{29}$ glassy alloy is single $(Co,Ta)_{23}B_6$ phase. With the increase of annealing temperature to 1073, $(Co,Ta)_{23}B_6$ phase partially decomposes to CoB and Co_4B phases. For the high B content $Co_{57}Ni_2Ta_6B_{35}$ glassy alloy with a single crystallization event, CoB and Co_4B phases precipitate synchronously and no $(Co,Ta)_{23}B_6$ was detected. By comparing the XRD patterns of different alloys annealed at 1073 K, we can find that the relative content and volume fraction of $(Co,Ta)_{23}B_6$ phase decrease and simple phases increase, with the increase of B content.

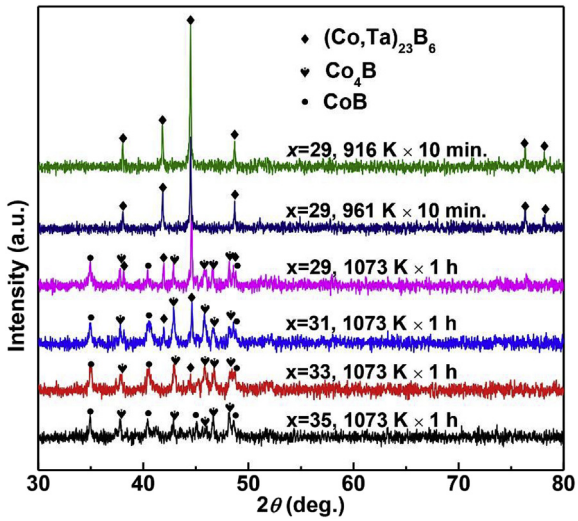

Fig. 9. XRD patterns of the annealed $Co_{92-x}Ni_2Ta_6B_x$ (x = 35, 33, 31, 29) ribbons.

Combined analysis of the B content dependence of B_s and the precipitation phases, it is easy for us to deduce that the $(Co,Ta)_{23}B_6$ phase is strong magnetic and the CoB and Co_4B phases are poor magnetic. The increase of B content can substantially improve the thermal stability of the glassy alloys and inhibit the formation of strong magnetic phases. The amorphization induced non-magnetic feature and magnetization decrease can be attributed to the amorphous distribution of Co atoms and poor magnetic interaction at glassy state. This structural transition is the basic mechanism for the development of nonmagnetic BMGs with ferromagnetic-element-based alloys.

The former results of precipitation phases and a process can also help us to understand the different glass-forming mechanisms of the $Co_{92-x}Ni_2Ta_6B_x$ (x = 35, 33, 31, 29) master alloys. The complicated structure of single primary precipitation phase and competing precipitation process of multiple phases are two typical and useful routes for high GFA. It has been well studied that the $(Co,Fe,Ni)_{23}B_6$ type phases have a complicated dense network structure of trigonal prisms connected through glue atoms like Ta and Nb etc [38]. The precipitation of the $(Co,Ta)_{23}B_6$ phase requires long-range atomic rearrangements and lead to a high thermal stability of the glassy phase against crystallization. For the alloys with low B content, the formation of $(Co,Ta)_{23}B_6$ phase with a complex structure is the reason for high GFA. For the high B content alloys, two simple phases in a single crystallization event will suffer stiff competition and inhibit mutually [39,40], leading to the high stability of supercooled liquid and high GFA. It is interesting to have two GFA enhancement mechanisms in one alloy

system and continuous compositions, requiring more in-depth investigations.

4. Conclusion

In this study, non-magnetic and ductile $Co_{92-x}Ni_2Ta_6B_x$ (x = 35, 33, 31, 29) BMGs were fabricated. Effects of B content on thermal properties, GFA, mechanical and magnetic properties were studied and the non-magnetic feature, crystallization behavior were discussed. These alloys exhibiting high thermal stability and GFA, superhigh hardness and strength, are promising coating materials for industrial applications. The main conclusions are as follows:

1) All $Co_{92-x}Ni_2Ta_6B_x$ (x = 35, 33, 31, 29) BMGs exhibit high T_g of 893–940 K and T_x of 916–980 K. Suitable adjustment of Co and B contents could improve the GFA, and BMG rods with a critical diameter of 1.5–2.5 mm were prepared.
2) The $Co_{92-x}Ni_2Ta_6B_x$ (x = 35, 33, 31, 29) BMGs possess excellent mechanical properties including ultra-high hardness of 1290–1410 HV, σ_y of 5.21–5.63 GPa and large plasticity up to 3.5%. The multiple shear bands and vein-like patterns were observed on the lateral and fraction surfaces which ensured the improved plasticity.
3) All $Co_{92-x}Ni_2Ta_6B_x$ (x = 35, 33, 31, 29) glassy ribbons exhibit the non-magnetic feature. The amorphization can effectively decrease the magnetization and lead to non-magnetic glassy alloys. Compared with the commonly used 304 stainless steel, the B_s of these Co-based BMGs is much lower, even for the high B alloy samples with partial crystallization.
4) A change of primary crystallization phase from complicated $(Co,Ta)_{23}B_6$ phase to simple phases were found in the $Co_{92-x}Ni_2Ta_6B_x$ (x = 35, 33, 31, 29) glassy alloys. The precipitation of the $(Co,Ta)_{23}B_6$ phase needing long-range atomic rearrangements is the reason of high GFA of low B content alloys. The competition induced mutual inhibition of two simple phases leads to a high stability of supercooled liquid and high GFA of high B content alloys.

Acknowledgements

This work was supported by the National Key Research and Development Program of China (Grant No. 2016YFB0300500), the National Natural Science Foundation of China (Grant No. 51774217, 51771159, 51601206). This research was also supported by the Hong Kong Government GRF funds (Grant No. CityU 11209314 and 11205515).

References

[1] M.M. Khan, A. Nemati, Z.U. Rahman, U.H. Shah, H. Asgar, W. Haider, Recent advancements in bulk metallic glasses and their applications: a review, Crit. Rev. Solid State Mater. Sci. 43 (3) (2018) 233–268.
[2] A. Wang, C. Zhao, A. He, H. Men, C. Chang, X. Wang, Composition design of high Bs Fe-based amorphous alloys with good amorphous-forming ability, J. Alloy. Comp. 656 (2016) 729–734.
[3] A. Inoue, B.L. Shen, H. Koshiba, H. Kato, A.R. Yavari, Cobalt-based bulk glassy alloy with ultrahigh strength and soft magnetic properties, Nat. Mater. 2 (10) (2003) 661–663.
[4] L. Chang, L. Xie, M. Liu, Q. Li, Y. Dong, C. Chang, X.-M. Wang, A. Inoue, Novel Fe-based nanocrystalline powder cores with excellent magnetic properties produced using gas-atomized powder, J. Magn. Magn Mater. 452 (2018) 442–446.
[5] S. Lee, H. Kato, T. Kubota, A. Makino, A. Inoue, Fabrication and soft-magnetic properties of Fe-B-Nb-Y glassy powder compacts by spark plasma sintering technique, Intermetallics 17 (4) (2009) 218–221.
[6] C. Zhang, L. Liu, K.C. Chan, Q. Chen, C.Y. Tang, Wear behavior of HVOF-sprayed Fe-based amorphous coatings, Intermetallics 29 (2012) 80–85.
[7] L.Q. Shen, Y.C. Hu, H.Y. Bai, Y.H. Sun, B.A. Sun, Y.H. Liu, W.H. Wang, Shear-band Affected Zone Revealed by Magnetic Domains in a Ferromagnetic Metallic Glass, (2018), https://doi.org/10.1038/s41467-018-06919-2.
[8] A. Inoue, B.L. Shen, H. Koshiba, H. Kato, A.R. Yavari, Ultra-high strength above 5000 MPa and soft magnetic properties of Co-Fe-Ta-B bulk glassy alloys, Acta Mater. 52 (6) (2004) 1631–1637.
[9] L. Liu, C. Zhang, Fe-based amorphous coatings: structures and properties, Thin Solid Films 561 (2014) 70–86.
[10] X. Li, A. Makino, H. Kato, A. Inoue, T. Kubota, Fe(76)Si(9.6)B(8.4)P(6) glassy powder soft-magnetic cores with low core loss prepared by spark-plasma sintering, Materials Science and Engineering B-Advanced Functional Solid-State Materials 176 (15) (2011) 1247–1250.
[11] Z. Yu, W. Jin-dong, Z. Yan-qin, Z. Yu, L. Xiao-wu, N. Hong-jun, Current situation of plasma spraying technology, Mod. Chem. Ind. 36 (6) (2016) 46–50.
[12] H.S. Choi, J. Kim, C. Lee, K.H. Lee, Critical factors affecting the amorphous phase formation of NiTiZrSiSn bulk amorphous feedstock in vacuum plasma spray, J. Mater. Sci. 40 (14) (2005) 3873–3875.
[13] H. Shiwen, L. Yong, G. Sheng, Cooling rate calculation of non-equilibrium aluminum alloy powders prepared by gas atomization, Rare Metal Mater. Eng. 38 (s1) (2009) 353–356.
[14] R. Highmore, A. Greer, Eutectics and the formation of amorphous alloys, Nature 339 (6223) (1989) 363–365.
[15] A. Inoue, A. Takeuchi, Recent development and application products of bulk glassy alloys, Acta Mater. 59 (6) (2011) 2243–2267.
[16] J.F. Wang, R. Li, N.B. Hua, T. Zhang, Co-based ternary bulk metallic glasses with ultrahigh strength and plasticity, J. Mater. Res. 26 (16) (2011) 2072–2079.
[17] J.F. Wang, L.G. Wang, S.K. Guan, S.J. Zhu, R. Li, T. Zhang, Effects of boron content on the glass-forming ability and mechanical properties of Co-B-Ta glassy alloys, J. Alloy. Comp. 617 (2014) 7–11.
[18] Y.Q. Dong, A.D. Wang, Q.K. Man, B.L. Shen, Co1-xFex, 68)B21.9Si5.1Nb5 bulk glassy alloys with high glass-forming ability, excellent soft-magnetic properties and superhigh fracture strength, Intermetallics 23 (2012) 63–67.
[19] A. Inoue, F.L. Kong, Q.K. Man, B.L. Shen, R.W. Li, F. Al-Marzouki, Development and applications of Fe- and Co-based bulk glassy alloys and their prospects, J. Alloy. Comp. 615 (2014) S2–S8.
[20] L.L. Shi, J. Xu, E. Ma, Alloy compositions of metallic glasses and eutectics from an idealized structural model, Acta Mater. 56 (14) (2008) 3613–3621.
[21] A. Inoue, Stabilization of metallic supercooled liquid and bulk amorphous alloys, Acta Mater. 48 (1) (2000) 279–306.
[22] A. Wang, C. Zhao, A. He, S. Yue, C. Chang, B. Shen, X. Wang, R.-W. Li, Development of FeNiNbSiBP bulk metallic glassy alloys with excellent magnetic properties and high glass forming ability evaluated by different criterions, Intermetallics 71 (2016) 1–6.
[23] S. Guo, Z.P. Lu, C.T. Liu, Identify the best glass forming ability criterion, Intermetallics 18 (5) (2010) 883–888.
[24] C.A. Schuh, T.G. Nieh, A nanoindentation study of serrated flow in bulk metallic glasses, Acta Mater. 51 (1) (2003) 87–99.
[25] B. Prakash, K. Hiratsuka, Sliding wear behaviour of some Fe-, Co- and Ni-based metallic glasses during rubbing against bearing steel, Tribol. Lett. 8 (2–3) (2000) 153–160.
[26] M.M. Trexler, N.N. Thadhani, Mechanical properties of bulk metallic glasses, Prog. Mater. Sci. 55 (2010) 759–839.
[27] B.A. Sun, W.H. Wang, The fracture of bulk metallic glasses, Prog. Mater. Sci. 74 (2015) 211–307.
[28] T. Mukai, T.G. Nieh, Y. Kawamura, A. Inoue, K. Higashi, Effect of strain rate on compressive behavior of a Pd40Ni40P20 bulk metallic glass, Intermetallics 10 (11–12) (2002) 1071–1077.
[29] C.J. Lee, J.C. Huang, T.G. Nieh, Sample size effect and microcompression of Mg65Cu25Gd10 metallic glass, Appl. Phys. Lett. 91 (16) (2007) 3.
[30] Y.J. Huang, J. Shen, J.F. Sun, Bulk metallic glasses: smaller is softer, Appl. Phys. Lett. 90 (8) (2007).
[31] Z.F. Zhang, J. Eckert, L. Schultz, Difference in compressive and tensile fracture mechanisms of Zr59CU20Al10Ni8Ti3 bulk metallic glass, Acta Mater. 51 (4) (2003) 1167–1179.
[32] Z.F. Zhang, G. He, J. Eckert, L. Schultz, Fracture mechanisms in bulk metallic glassy materials, Phys. Rev. Lett. 91 (4) (2003) 045505.
[33] S.V. Madge, Toughness of bulk metallic glasses, Metals 5 (3) (2015) 1279–1305.
[34] Y.T. Wang, X.K. Xi, G. Wang, X.X. Xia, W.H. Wang, Understanding of nanoscale periodic stripes on fracture surface of metallic glasses, J. Appl. Phys. 106 (11) (2009) 113528.
[35] M. Zhang, A. Wang, B. Shen, Enhancement of glass-forming ability of Fe-based bulk metallic glasses with high saturation magnetic flux density, AIP Adv. 2 (2) (2012) 022169-7.
[36] H.W. Sheng, W.K. Luo, F.M. Alamgir, J.M. Bai, E. Ma, Atomic packing and short-to-medium-range order in metallic glasses, Nature 439 (7075) (2006) 419–425.
[37] X.J. Gu, S.J. Poon, G.J. Shiflet, M. Widom, Ductility improvement of amorphous steels: roles of shear modulus and electronic structure, Acta Mater. 56 (1) (2008) 88–94.
[38] M. Imafuku, S. Sato, H. Koshiba, E. Matsubara, A. Inoue, Structural variation of Fe-Nb-B metallic glasses during crystallization process, Scripta Mater. 44 (8–9) (2001) 2369–2372.
[39] M.X. Xia, S.G. Zhang, C.L. Ma, J.G. Li, Evaluation of glass-forming ability for metallic glasses based on order-disorder competition, Appl. Phys. Lett. 89 (9) (2006) 091917.
[40] P. Jalali, M. Li, Competing microstructure and crystalline phase formation and their roles in glass formability: a molecular dynamics study, Intermetallics 12 (10–11) (2004) 1167–1176.